LASER & PHOTONICS REVIEWS
www.lpr-journal.org

Circulator-Free Brillouin Photonic Planar Circuit

Yang Liu, Amol Choudhary, Guanghui Ren, Duk-Yong Choi, Alvaro Casas-Bedoya, Blair Morrison, Pan Ma, Thach G. Nguyen, Arnan Mitchell, Stephen J. Madden, David Marpaung, and Benjamin J. Eggleton**

On-chip stimulated Brillouin scattering (SBS) that results from enhanced light–sound interactions, has recently demonstrated great applicability and versatility for signal generation and manipulation. Progress toward realizing fully integrated Brillouin photonic circuits is promising; however, the control and routing of on-chip optical waves requires non-reciprocal elements such as circulators, which is challenging and adds complexity. Here, a circulator-free Brillouin photonic planar waveguide circuit which eliminates the need for separate non-reciprocal elements is demonstrated. Backward inter-modal Brillouin scattering (BIBS) is used in a planar photonic integrated circuit, for the first time, to provide Brillouin processing capability in a multi-modal waveguide, conveniently allowing for the separation of counter-propagating pump and signal using passive integrated mode-selective filters. Using an As_2S_3–Si hybrid multi-modal photonic circuit, inter-optical-mode energy transfer with a Brillouin gain coefficient of 280 $m^{-1}W^{-1}$ is experimentally demonstrated, representing two orders of magnitude enhancement compared to conventional optical fibers. This on-chip BIBS circuit allows for independent routing of pump and signal waves, showing resilience to the cross talk. The experimental demonstrations provide an important basis for achieving fully integrated Brillouin photonic circuits without requiring on-chip circulators and fine spectral filtering, opening a new dimension for studying spatial-dependent photon–phonon nonlinear dynamics.

1. Introduction

Stimulated Brillouin scattering (SBS) is an optomechanical interaction that originates from coherent nonlinear coupling between optical waves and sound waves.[1] SBS has been widely investigated in bulk media[2,3] and optical fibers,[4–6] and has underpinned a wide range of important applications, based on the unique nature of high-efficiency parametric (de)amplification and the ultra-fine spectral selectivity.[7] Recent advances in inducing and harnessing Brillouin scattering in centimeter-scale photonic chips[8–15] have enabled enhanced functionalities and advanced signal processing capability[16–18] for signal synthesis,[19,20] microwave photonic processing,[21–23] optical communication carrier regeneration,[24] signal storage,[25,26] and ultra-sensitive detection.[27] New hybrid integration approaches allow for the co-integration of lasers,[28] modulators,[29] detectors[30] and functional processing units,[22,31] providing the basis of a fully integrated Brillouin photonic chip that incorporates

Dr. Y. Liu[+], Dr. A. Casas-Bedoya, Dr. B. Morrison, Prof. B. J. Eggleton
Institute of Photonics and Optical Science (IPOS)
School of Physics
The University of Sydney
NSW 2006, Australia
E-mail: yang.liu@sydney.edu.au; benjamin.eggleton@sydney.edu.au

Dr. Y. Liu[+], Dr. A. Casas-Bedoya, Dr. B. Morrison, Prof. B. J. Eggleton
The University of Sydney Nano Institute (Sydney Nano)
The University of Sydney
NSW 2006, Australia

[+]Present address: Laboratory of Photonics and Quantum Measurements, Swiss Federal Institute of Technology Lausanne (EPFL), Lausanne, Switzerland

DOI: 10.1002/lpor.202000481

Prof. A. Choudhary
UltraFast Optical Communications and High-performance Integrated Photonics (UFO-CHIP)
Department of Electrical Engineering
Indian Institute of Technology (IIT) Delhi
Hauz Khas, New Delhi 110016, India

Dr. G. Ren, Dr. T. G. Nguyen, Prof. A. Mitchell
Integrated Photonics and Applications Centre (InPAC)
School of Engineering
RMIT University
VIC 3001, Australia

Prof. D.-Y. Choi, Dr. P. Ma, Prof. S. J. Madden
Laser Physics Centre
Australian National University
Canberra, ACT 2601, Australia

Prof. D. Marpaung
Nonlinear Nanophotonics Group
Laser Physics and Nonlinear Optics (LPNO)
University of Twente
Enschede, NB 7522, The Netherlands

Brillouin-active elements with functional photonic circuits, essential for enabling compact and robust signal processing systems.

Realizing fully integrated Brillouin photonic circuits requires the separation of pump and signal waves after Brillouin interactions, in order to avoid crosstalk and to protect critical devices such as lasers and photodetectors. Conventionally, the control and management of counter-propagating pump and signals for on-chip backward SBS devices requires off-chip circulators and fine-resolution filters, which spatially separate these closely spaced wavelengths on the basis of their propagation directions and wavelength, respectively. Although there has been good progress in the development of on-chip broadband optical circulators, the additional complexity of integrating magneto-optic materials and the need for off-chip excitation of magnetic fields[30,32] can be prohibitive. On-chip Brillouin-based active non-reciprocal elements[33,34] are promising but current approaches require suspended silicon membranes that compromise device robustness, and the intrinsic optical nonlinear loss of silicon limits achievable Brillouin gain in single-pass waveguides.[35,36] Therefore, a passive and simple approach, which allows for the separation of pump and signal waves without the need for on-chip circulators and high-resolution filters is highly desirable.

In this paper we report the first demonstration of on-chip backward inter-modal Brillouin scattering (BIBS), as the basis of a circulator-free multi-modal Brillouin circuit. In a hybrid As_2S_3-Si photonic planar chip, integrated silicon multiplexers can excite separate optical modes for the pump and signal waves in an As_2S_3 planar waveguide for BIBS process, which allows for inter-modal Brillouin amplification and energy transfer without nonlinear loss. The pump and signal waves are then separated by the silicon mode-selective filters to independent ports. The fabricated BIBS photonic circuit has reduced susceptibility to signal crosstalk caused by pump reflection due to the spatial separation of the input/output ports for signal and pump waves. This work makes an important step toward monolithically integrated Brillouin photonic systems by eliminating the need for complex and challenging circulators and fine-resolution filters, and also provides a new platform for exploring mode-dependent photon–phonon interaction dynamics.

2. Results

Figure 1 shows a conventional Brillouin photonic circuit and the circulator-free Brillouin circuit based on BIBS. A pair of off-chip optical circulators is usually required in the conventional scheme, as shown in Figure 1a. In contrast, in the proposed scheme, the optical signal in a fundamental mode injected via Port 4 is converted to a higher-order optical mode using a modal multiplexer, which is subsequently coupled to the multi-modal Brillouin-active waveguide, as show in Figure 1b. At the other end, the optical pump injected via Port 1 stays in the fundamental mode all the way through the entire circuit and exits the chip via Port 3. The BIBS process occurs in the Brillouin-active waveguide; the pump in the fundamental mode amplifies the counter-propagating signal in the higher-order mode. The amplified signal wave is then converted back to the fundamental optical mode using a modal demultiplexer and exits via Port 2. In

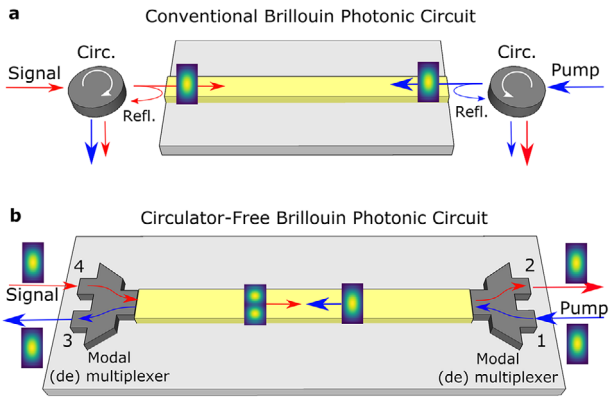

Figure 1. Concept and comparison of a) a conventional Brillouin photonic circuit that accommodates pump and signal in the same optical mode, and b) a circulator-free Brillouin photonic circuit that involves two distinct optical modes. For illustration purpose, transverse-electric (TE) modes, that is, TE_0 and TE_1 are used to illustrate the scheme of a circulator-free integrated Brillouin photonic circuit. Circ, optical circulator; Refl, reflection.

this process, well-established photonic integrated mode-selective devices[37,38] conveniently separate the transmitted pump and signal waves, based on their distinct mode properties. Moreover, the signal crosstalk can be well suppressed, since the injection and extraction of pump and signal waves uses spatially separated ports.

Figure 2 illustrates the principle of the BIBS process, where two distinct optical modes (one symmetric denoted in solid blue and one anti-symmetric in dashed red) are represented by two different dispersion curves in both, the forward and backward directions. Here, we focus on the illustration of BIBS between first two orders of optical modes, for the sake of clarity. We assume that a CW optical pump wave in the lower-order optical mode (symmetric type) propagates in the forward direction at frequency ω_p. An acoustic wave with matched wave vector and frequency can mediate the coupling between a signal wave $\omega_{s,1}$ in a higher-order optical mode (anti-symmetric type) and the pump wave (symmetric type). This inter-modal coupling forms the basis of the BIBS process that enables energy transfer between two different optical modes; this is in contrast to the conventional backward SBS (intra-modal BSBS) process involving two identical optical modes, as shown in Figure 2a. Due to the wave vector difference between the two distinct optical modes, the wave vector of the acoustic wave mediating the BIBS process differs from that of the intra-modal SBS processing. As a result, the BIBS process produces a Stokes gain resonance at a different frequency from that of the conventional intra-modal SBS, as shown in Figure 2b. The resultant gain coefficient of BIBS depends on the three-wave field overlap. Although pioneering demonstrations of BIBS process have been made in a micro-sphere cavity,[39] in few-modal fibers[40,41] and recently achieved in single-modal optical fibers between the core mode and the cladding mode,[42] it has not yet been well explored in integrated photonic platforms.[43] Forward inter-modal Brillouin scattering between co-propagating optical waves was reported in micro-structured fibers,[44] and was recently demonstrated in suspended silicon membrane photonic circuits[36] which enabled an isolator[34] and a silicon Brillouin laser.[45] While suspended devices have yielded

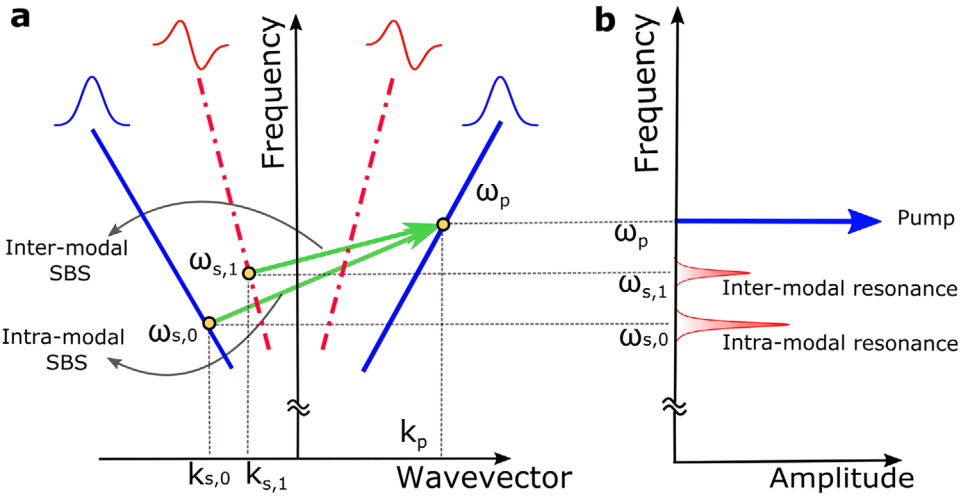

Figure 2. The principle of BIBS process. a) The dispersion diagram and b) spectral responses of inter-modal and intra-modal Brillouin scattering processes.

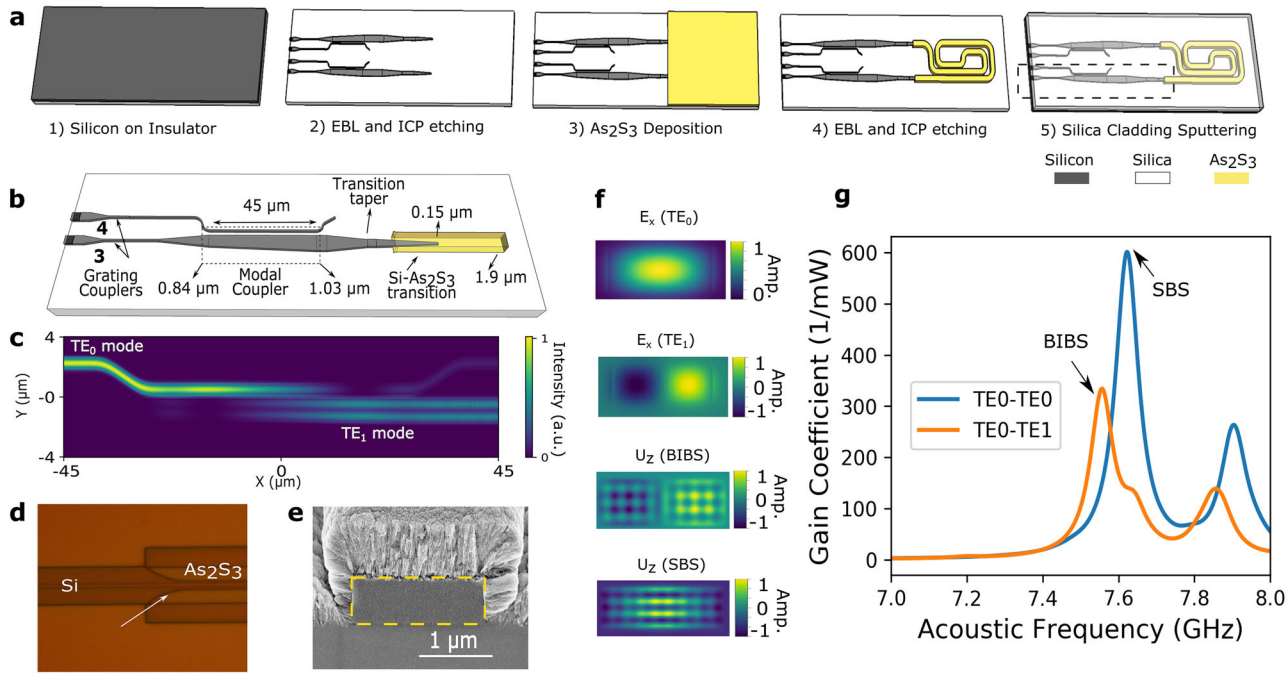

Figure 3. Design, fabrication and simulation for the circulator-free Brillouin photonic circuit. a) Fabrication process illustration, b) the schematic of the hybrid section consisting of a silicon modal multiplexer and a multi-modal As_2S_3 Brillouin waveguide outlined by the dashed box in (a). c) Simulated optical intensity (top view) in the silicon mode (de)multiplexer illustrated in (b). d) The optical image of the hybrid section where the silicon waveguide is overlaid with the As_2S_3 waveguide. e) The scanning electron microscopy image of fabricated multi-modal As_2S_3 waveguide cross section. f) The calculated dominant electric field component (E_x) of the optical TE_0 mode and the optical TE_1 mode, as well as the dominant longitudinal displacement (U_z) of the acoustic modes for the BIBS and SBS process, respectively. g) Calculated gain coefficients of BIBS and conventional SBS. EBL, electron beam lithography; ICP, inductively coupled plasma.

attractive features, they add fabrication constraints to the development and robustness of complex photonic–phononic circuits and systems.

Figure 3a shows the schematic and the fabrication process of the proposed integrated BIBS photonic circuit (see Section 4). Silicon mode (de)multiplexers and As_2S_3 multi-modal Brillouin waveguide are simultaneously integrated using the As_2S_3-Si hybrid integration technology.[31,46] Two identical silicon modal couplers are connected to the input and output of a spiral shaped multi-modal As_2S_3 Brillouin waveguide. The silicon grating couplers (partially etched) are oriented toward one side in an arrayed arrangement with a pitch of 127 μm, which allow for the light input and output coupling using a fiber array. The minimum total coupling loss of the hybrid BIBS device is 18.8 dB, including

an average coupling loss of 13.5 dB introduced by a pair of silicon grating couplers. For future applications, the input and output ports can directly interface with extended silicon photonic circuits via single-modal silicon waveguides.

The multi-modal output of the silicon multiplexer is tapered to a width of 0.15 μm for adiabatic light coupling in the As_2S_3-Si overlay region, as shown in Figure 3b. The mechanism of the silicon mode (de)multiplexer is illustrated by the numerical simulation of mode coupling in Figure 3c. The fundamental optical TE_0 mode in the narrower waveguide (the upper arm) is efficiently coupled to the higher-order TE_1 mode in the wide waveguide (the lower arm), due to the phase matching of effective refractive indices of the TE_0 and TE_1 modes in the coupling area. Similarly, the TE_1 mode in the wider waveguide can be coupled to the TE_0 in the narrow waveguide with the same coupling efficiency, when TE_1 propagating reversely in the silicon modal coupler due to its linear reciprocal optical property. In contrast, the TE_0 mode in the wide silicon waveguide remains in the same mode, due to the effective refractive index mismatching with other optical modes. The silicon mode coupler is numerically designed to achieve the mode conversion from TE_0 mode via Port 4 to TE_1 in the tapered silicon multi-modal waveguide with a conversion efficiency of −0.5 dB. Due to the tapered multi-modal waveguide design, the mode conversion crosstalk can be suppressed to be less than −40 dB. We utilized curved interfaces to release the tensile stress to avoid causing cracks along the As_2S_3 waveguide, as shown in Figure 3d. As_2S_3-Si overlay region produces negligible mode transition loss for TE_0 mode and <0.4 dB loss for TE_1, respectively; less than −19 dB of the mode power will be converted to other higher-order optical modes, according to numerical simulations. Figure 3e shows the cross section (outlined by dashed box) of the As_2S_3 strip waveguide with a designed dimension of 1900 nm ×680 nm on a buried oxide substrate with low-temperature sputtered silica upper cladding. The columnar feature in the silica upper cladding leads to a measured optical propagation loss of around 1 dB cm^{-1} for the fundamental optical mode; the loss can be reduced using ion beam sputtering technique that provides a higher quality of silica cladding sputtering. The overall propagation loss of the TE_1 mode is around 3.5 dB cm^{-1} including the contribution from bending loss. Although in principle this BIBS circuit can be implemented using pure As_2S_3 planar waveguides,[22] the fabrication of 150 nm wide gap in 700 nm thick As_2S_3 film for modal couplers is challenging due to the high aspect ratio for etching.

Figure 3f shows the dominant field components of simulated optical modes (TE_0 and TE_1 modes) accommodated in the multi-modal As_2S_3, with an effective refractive index of 2.27 and 2.17, respectively. This strip waveguide is highly birefringent due to the rectangular cross section, and thus we mainly consider the TE polarized optical modes that can maintain the polarization while propagating in the waveguide. Using a full-vectorial finite element analysis approach,[47] the dominant longitudinal displacement of the acoustic mode that mediates the BIBS process is shown in Figure 3f (1900 nm ×680 nm As_2S_3 waveguide core buried in silica); the acoustic displacement represents a measurement of distance of the movement of medium with unit volume from its equilibrium position. The acoustic mode for BIBS can yield a non-zero integral field overlap with the two optical modes, producing a decent Brillouin gain. In comparison, the dominant acoustic mode for conventional SBS process shows a symmetric field distribution. The acoustic displacement component (U_z) exhibits complex field distribution due to the As_2S_3 waveguide is heavily multi-modal for acoustic waves. The numerical calculation shown in Figure 3g indicates a dominant BIBS gain coefficient of 320 $m^{-1}W^{-1}$ in the designed multi-modal As_2S_3 waveguide, which is about half of the gain coefficient of the conventional intra-modal SBS in the Brillouin waveguides with same dimensions. The full width at half maximum (FWHM) linewidth (≈30 MHz) of the BIBS is similar to that of the conventional inter-modal SBS process. The reduced gain coefficient mainly results from the decreased field overlap of TE_0 and TE_1 modes for the BIBS process, compared to the case of intra-modal SBS with two identical TE_0 modes, as shown in Figure 3f. A few weaker gain peaks exist in the calculated responses, originating from acoustic modes that have non-zero overlap with the optical modes. The calculated Brillouin frequency shift (BFS) of BIBS is ≈65 MHz lower than that of intra-modal SBS, owing to the reduced acoustic wave vector. The difference in BFS can be controlled by engineering the effective refractive indices of optical modes. It should be noted that BIBS process can be induced between other optical TE modes, transverse-magnetic (TM) modes, and distinct polarized optical modes, once the symmetry properties of optical fields and acoustic field allows for non-zero integral overlap.[48]

We proceed to investigate the BIBS process in the fabricated hybrid Brillouin photonic chip using the experimental setup illustrated in **Figure 4**a (see Section 4). The pump wave and signal wave are directly coupled to the chip through Port 1 and Port 4, respectively, without using any non-reciprocal optical devices such as circulators; this configuration is in contrast to the setup for conventional backward SBS. This important advantage is offered by the combination of the BIBS process and the mode-selective devices. We experimentally evaluated the Brillouin gain coefficient of BIBS in order to verify the simulations shown in in Figure 3f. Figure 4b shows the measured Stokes responses of BIBS (TE_1-TE_0) and the conventional SBS (TE_0-TE_0) in a hybrid photonic chip with a 1.9-cm-long As_2S_3 waveguide, under a constant coupled on-chip pump power of ≈100 mW. The BIBS exhibits a gain of resonance with a Brillouin frequency shift (BFS) of 7.585 GHz, while the intra-modal SBS shows a higher BFS of 7.645 GHz. In the measurement for the conventional intra-modal SBS, off-chip fiber-based optical circulators were inserted between the generated pump/signal waves and the chip, coupled through using Port 1 and Port 2, respectively. As illustrated in Figure 2, the difference in BFS is due to the distinct wave numbers of acoustic waves participating in the BIBS process and the intra-modal SBS, which demonstrates the generation of BIBS in the hybrid As_2S_3-Si photonic chip. The measured Brillouin gain is mainly limited by the relatively high optical propagation losses due to the roughness of silica upper cladding with columnar structures and tight waveguide bends.

By fitting the measured results shown in Figure 4c, the Brillouin scattering from TE_0 mode to TE_1 BIBS has a Brillouin gain coefficient of 280 $m^{-1}W^{-1}$, which shows an enhancement of about 300 times compared to that measured in few-modal optical fibers.[41] The two order of magnitude enhancement is achieved due to the tightly confinement of optical and acoustic waves in

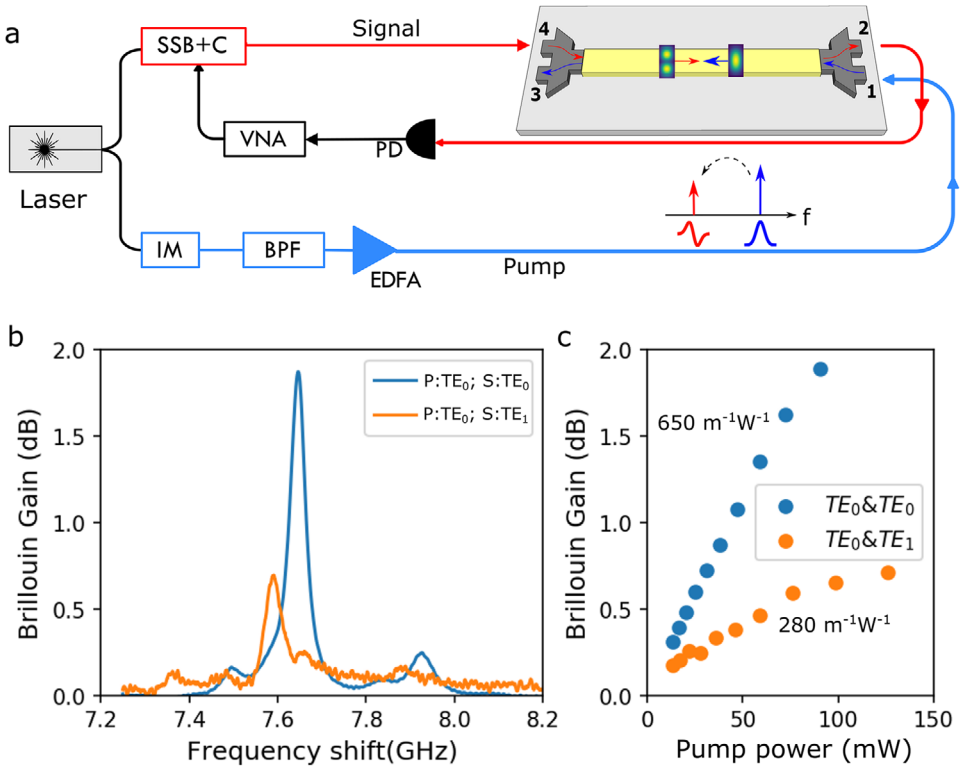

Figure 4. Experimental demonstration of the circulator-free Brillouin photonic circuit. a) Experimental setup and configuration. Measured b) on/off Brillouin Stokes responses of BIBS and conventional SBS under 100 mW optical pump power, and c) gain as a function of coupled pump power in a hybrid chip with a 1.9-cm-long As_2S_3 waveguide. SSB+C, single-sideband modulation with carrier; VNA, vector network analyzer; PD, photodetector; IM, intensity modulation; BPF, optical bandpass filter; EDFA, erbium-doped fiber amplifier.

wavelength-scale photonic waveguides. The measurements are well matched with the numerical calculations shown in Figure 3f, in comparison with conventional intra-modal Brillouin scattering (650 $m^{-1}W^{-1}$) between two identical TE_0 modes measured in the same chip. The difference in gain coefficients is due to the fact that the integral field overlap of the symmetric (TE_0) and the anti-symmetric (TE_1) modes in BIBS is smaller than that of two TE_0 modes in the intra-modal SBS process, according to the simulated optical and acoustic fields shown in Figure 3f. The measured gain coefficient indicates that the BIBS process in the hybrid chip can yield appreciable Brillouin gain in centimeter-long waveguides for signal generation and processing applications, while sustaining reduced complexity and footprint.

The BIBS interaction can also enable the energy transfer from a higher-order optical mode to a lower-order optical mode, in a reverse fashion to the scheme shown in Figure 2a. In experiment, we swapped the order of the optical modes of the pump and the signal by switching the input ports, that is, from Port 1 to Port 2 for pump, and from Port 4 to Port 3 for signal, respectively. Therefore, the pump wave is coupled to the TE_1 mode, while the signal wave stays in the TE_0 mode in a 8-mm-long As_2S_3 waveguide. We switched to this shorter hybrid BIBS waveguide due to the sample availability during experiments. The applied pump power is currently limited by the damage threshold of the silicon grating couplers, which can be further increased using materials and structures with a higher power handling capability. **Figure 5**a shows the measured Stokes and anti-Stokes

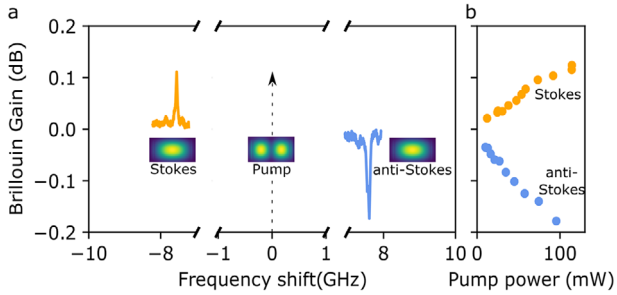

Figure 5. Demonstration of two-way energy transfer between distinct optical modes using the hybrid BIBS photonic circuit. Insets show the calculated optical modes in the hybrid chip.

responses of the BIBS process, when the pump (100 mW) is carried by a higher-order optical mode (TE_1). The measured gain resonance at the Stoke frequency indicates that the energy in the higher-order optical mode (TE_1) is transferred to the lower-order optical mode (TE_0), while the loss resonance at the anti-Stokes frequency reveals an energy flow from the TE_0 mode to the TE_1 mode. The measured Brillouin amplification (de-amplification) is mainly limited by the short (8 mm) As_2S_3 waveguide length. One can note that the Stokes process of BIBS in Figure 5b shows saturation at a power pump power around 80 mW due to the higher loss of the optical pump and the limited waveguide length. Figure 5b also shows the parametric energy transfer as a function

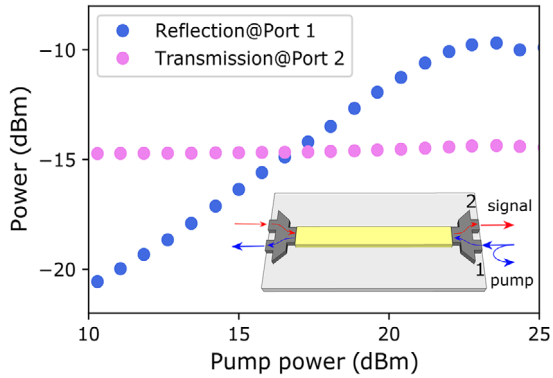

Figure 6. Measured optical powers of reflected pump at Port 1 and transmitted signal at Port 2. BIBS chip shows the robustness to signal crosstalk caused by pump reflection, compared to the conventional Brillouin circuit scheme.

of the pump power for the Stokes and anti-Stokes components, respectively. The slight difference in the gain slope for Stokes and anti-Stokes at a pump power of >50 mW is due to the measurement uncertainty in the small signal detection. These measurements indicate that the BIBS process can achieve controllable energy transfer between two distinct optical modes, which implies a great potential for amplifying and filtering of signals in distinct mode channels in on-chip mode-division multiplexing systems.

The proposed hybrid BIBS chip can avoid the signal crosstalk between the probe and pump waves, since the input and output ports for pump and signal waves are spatially separated. **Figure 6** shows that the transmitted signal (off resonance) at Port 2 stays unaffected. In contrast, the pump reflection (measurement assisted by an off-chip circulator) increases as the pump power ramps up by >15 dB. This crosstalk mitigation capability is unattainable in conventional SBS schemes where the pump and signal waves share the same input and output ports. We note that the roll-off in pump reflection at high powers is due to the thermal-induced coupling drifting in fiber-to-chip coupling and is not due to nonlinear loss in the waveguide.

3. Conclusion

The demonstration of on-chip BIBS and its attractive advantages in signal manipulation and crosstalk reduction present an important technical step forward, providing a promising solution to eliminating the need of complex and challenging on-chip devices to control and route optical signals. Although the immediate application of the on-chip BIBS in signal processing, amplification and signal generation is currently constrained by the limited Brillouin gain, several feasible improvements can be made to significantly increase the achievable gain by reducing the optical losses to <1 dB cm^{-1} level, through using improved etching process to reduce the waveguide sidewall scattering loss, as well as deploying larger and optimized multi-modal bends to avoid additive mode conversion loss.[49] Thus, it is possible to achieve >20 dB BIBS gain and net signal gain in single-pass waveguides, which is desirable for practical applications. This level of foreseeable performance will compete and possibly overtake the demonstrated single-digit Brillouin using forward SBS in ultra-loss silicon suspended waveguide[35,36] that is currently limited by the silicon nonlinear losses and the achievable waveguide length. The recent emergence of on-chip surface acoustic wave (SAW) transducers[11,50] provides a promising way to efficiently excite acoustic waves in integrated photonic circuits, without requiring complex waveguide structures or hybrid material integration.[51,52] Among these reported, the recent electrically driven approach utilizing a non-suspended silicon waveguides promises a flexible control of photon–phonon interaction without the need of optical pump to excite acoustic waveguides, which provides an alternative technique to facilitate advanced Brillouin-based applications.

In conclusion, we have demonstrated a novel integrated Brillouin photonic circuit that allows for direct interfacing and integration with well-established photonic integrated circuits, without using on-chip or off-chip optical circulators. This is achieved by leveraging the Brillouin scattering between different spatial optical modes and mode-selective filtering, in an integrated hybrid As_2S_3-Si photonic circuit platform. This scheme simultaneously enables multi-fold advantages including inter-modal nonlinear energy transfer with a Brillouin gain coefficient of 280 $m^{-1}W^{-1}$, pump and signal routing without using on-chip circulator, and reduced susceptibility to the crosstalk caused by pump reflections. This demonstrated scheme is an important step to achieving monolithically integrated Brillouin photonic processors and provides a novel platform to explore inter-modal light–sound interaction dynamics.

4. Experimental Section

Sample Fabrication: Firstly, a base silicon circuit including silicon mode (de)multiplexers, grating couplers, and tapered silicon nanowires (see detailed dimensions in Figure 3b) was fabricated, using electron beam lithography (EBL) and inductively coupled plasma (ICP) etching to pattern the fully etched silicon modal couplers. Subsequently, an amorphous As_2S_3 film was thermally deposited in a targeted open region next to the silicon tapered nanowires using a shadow mask. Optical and thermal annealing was used to stabilize the refractive index of As_2S_3 at n = 2.44 at the wavelength of 1550 nm. Then, the As_2S_3 multi-modal strip waveguides were fabricated using EBL and ICP dry etching in an Oxford Plasmalab 100 ICP RIE system using a mixture of CHF_3, O_2, and Ar gases. Finally, a SiO_2 upper-cladding with a thickness of 1 µm was deposited via the low-pressure sputtering process.

Experimental Measurement: One portion of a laser was modulated using a dual-parallel Mach–Zehnder modulator (DPMZM), to generate a single-sideband optical signal, as shown in Figure 4a. The sideband frequency was linearly swept over frequency range that covers the BIBS-induced resonances, while the optical carrier serves as an optical oscillator that provides heterodyne measurement with the sweeping sideband in photodetection. This single-sideband signal was injected into the photonic chip via Port 4, and was subsequently coupled into the multi-modal As_2S_3 waveguide. The other tap of the laser output was modulated by an intensity modulator which generates two optical sidebands; an optical bandpass filter selected the higher sideband as the optical pump wave. The optical pump wave was amplified by an erbium-doped fiber amplifier, before being sent to the chip via Port 1. The optical sideband of the probe signal was amplified (or de-amplified) by the pump in TE_0 mode via the BIBS process. The output probe signal exited the chip via Port 2. The processed probe signal was coupled out of the chip through Port 3 and then collected by a photodetector. An electrical vector network analyzer mapped the SBS response to the RF domain.

Acknowledgements

This work was supported by Lockheed Martin under the University of Sydney contract, Australian Research Council (ARC) 2020 Discovery Project (DP200101893), and Science and Engineering Research Board (SERB), project: SRG/2019/001632. The authors would like to acknowledge the facilities, and the scientific and technical assistance of the Micro Nano Research Facility (MNRF) at RMIT University. This work was performed in part at the Melbourne Centre for Nanofabrication (MCN) in the Victorian Node of the Australian National Fabrication Facility (ANFF).

Conflict of Interest

The authors declare no conflict of interest.

Data Availability Statement

The data that support the findings of this study are available from the corresponding author upon reasonable request.

Keywords

Brillouin scattering, integrated photonics, inter-modal optical nonlinearity, nonlinear optics

Received: October 31, 2020
Revised: January 12, 2021
Published online: March 18, 2021

[1] G. P. Agrawal, *Nonlinear Fiber Optics*, Academic Press, New York **2007**.
[2] R. Y. Chiao, B. P. Stoicheff, *J. Opt. Soc. Am.* **1964**, *54*, 1286.
[3] R. Brewer, K. Rieckhoff, *Phys. Rev. Lett.* **1964**, *13*, 334.
[4] E. Ippen, R. Stolen, *Appl. Phys. Lett.* **1972**, *21*, 539.
[5] J.-C. Beugnot, S. Lebrun, G. Pauliat, H. Maillotte, V. Laude, T. Sylvestre, *Nat. Commun.* **2014**, *5*, 5242.
[6] M. Nikles, L. Thevenaz, P. Robert, *J. Lightwave Technol.* **1997**, *15*, 1842.
[7] A. Kobyakov, M. Sauer, D. Chowdhury, *Adv. Opt. Photon.* **2010**, *2*, 1.
[8] B. J. Eggleton, C. G. Poulton, P. T. Rakich, M. J. Steel, G. Bahl, *Nat. Photonics* **2019**, *13*, 664.
[9] A. H. Safavi-Naeini, D. Van Thourhout, R. Baets, R. Van Laer, *Optica* **2019**, *6*, 213.
[10] ÇS., P. Dainese, T. P. Alegre, *APL Photonics* **2019**, *4*, 7.
[11] Q. Liu, H. Li, M. Li, *Optica* **2019**, *6*, 778.
[12] A. Choudhary, B. Morrison, I. Aryanfar, S. Shahnia, M. Pagani, Y. Liu, K. Vu, S. Madden, D. Marpaung, B. J. Eggleton, *J. Lightwave Technol.* **2017**, *35*, 846.
[13] R. Pant, C. G. Poulton, D.-Y. Choi, H. McFarlane, S. Hile, E. Li, L. Thevenaz, B. Luther-Davies, S. J. Madden, B. J. Eggleton, *Opt. Express* **2011**, *19*, 8285.
[14] H. Shin, W. Qiu, R. Jarecki, J. A. Cox, R. H. Olsson, A. Starbuck, Z. Wang, P. T. Rakich, *Nat. Commun.* **2013**, *4*, 1944.
[15] R. Van Laer, B. Kuyken, D. Van Thourhout, R. Baets, *Nat. Photonics* **2015**, *9*, 199.
[16] M. Merklein, A. Casas-Bedoya, D. Marpaung, T. F. S. Buttner, M. Pagani, B. Morrison, I. V. Kabakova, B. J. Eggleton, *IEEE J. Sel. Top. Quantum Electron.* **2016**, *22*, 336.
[17] A. Choudhary, Y. Liu, D. Marpaung, B. J. Eggleton, *IEEE J. Sel. Top. Quantum Electron.* **2018**, *24*, 1.
[18] Y. Liu, A. Choudhary, D. Marpaung, B. J. Eggleton, *IEEE J. Quantum Electron.* **2018**, *54*, 3.
[19] J. Li, H. Lee, K. J. Vahala, *Nature Commun.* **2013**, *4*, 2097.
[20] S. Gundavarapu, G. M. Brodnik, M. Puckett, T. Huffman, D. Bose, R. Behunin, J. Wu, T. Qiu, C. Pinho, N. Chauhan, J. Nohava, P. T. Rakich, K. D. Nelson, M. Salit, D. J. Blumenthal, *Nat. Photonics* **2019**, *13*, 60.
[21] D. Marpaung, B. Morrison, M. Pagani, R. Pant, D.-Y. Choi, B. Luther-Davies, S. J. Madden, B. J. Eggleton, *Optica* **2015**, *2*, 76.
[22] Y. Liu, A. Choudhary, G. Ren, K. Vu, B. Morrison, A. Casas-Bedoya, T. G. Nguyen, D. Y. Choi, P. Ma, A. Mitchell, S. J. Madden, D. Marpaung, B. J. Eggleton, *APL Photonics* **2019**, *4*, 10.
[23] Y. Liu, A. Choudhary, D. Marpaung, B. J. Eggleton, *Adv. Opt. Photonics* **2020**, *12*, 485.
[24] E. Giacoumidis, A. Choudhary, E. Magi, D. Marpaung, K. Vu, P. Ma, D.-Y. Choi, S. Madden, B. Corcoran, M. Pelusi, B. J. Eggleton, *Optica* **2018**, *5*, 1191.
[25] M. Merklein, B. Stiller, K. Vu, S. J. Madden, B. J. Eggleton, *Nat. Commun.* **2017**, *8*, 1.
[26] B. Stiller, M. Merklein, C. Wolff, K. Vu, P. Ma, S. Madden, B. Eggleton, *Optica* **2020**, *7*, 5.
[27] Y. H. Lai, M. G. Suh, Y. K. Lu, B. Shen, Q. F. Yang, H. Wang, J. Li, S. H. Lee, K. Y. Yang, K. Vahala, *Nat. Photonics* **2020**, *14*, 398.
[28] C. Xiang, W. Jin, J. Guo, J. D. Peters, M. J. Kennedy, J. Selvidge, P. A. Morton, J. E. Bowers, *Optica* **2020**, *7*, 20.
[29] M. He, M. Xu, Y. Ren, J. Jian, Z. Ruan, Y. Xu, S. Gao, S. Sun, X. Wen, L. Zhou, L. Liu, C. Guo, H. Chen, S. Yu, L. Liu, X. Cai, *Nat. Photonics* **2019**, *13*, 359.
[30] Z. Su, E. S. Hosseini, E. Timurdogan, J. Sun, M. Moresco, G. Leake, T. N. Adam, D. D. Coolbaugh, M. R. Watts, *Opt. Lett.* **2017**, *42*, 2878.
[31] B. Morrison, A. Casas-Bedoya, G. Ren, K. Vu, Y. Liu, A. Zarifi, T. G. Nguyen, D.-Y. Choi, D. Marpaung, S. J. Madden, A. Mitchell, B. J. Eggleton, *Optica* **2017**, *4*, 847.
[32] L. Bi, J. Hu, P. Jiang, D. H. Kim, G. F. Dionne, L. C. Kimerling, C. A. Ross, *Nat. Photonics* **2011**, *5*, 758.
[33] C. G. Poulton, R. Pant, A. Byrnes, S. Fan, M. J. Steel, B. J. Eggleton, *Opt. Express* **2012**, *20*, 21235.
[34] E. A. Kittlaus, N. T. Otterstrom, P. Kharel, S. Gertler, P. T. Rakich, *Nat. Photonics* **2018**, *12*, 613.
[35] E. A. Kittlaus, H. Shin, P. T. Rakich, *Nat. Photonics* **2016**, *10*, 463.
[36] E. A. Kittlaus, N. T. Otterstrom, P. T. Rakich, *Nat. Commun.* **2017**, *8*, 15819.
[37] Y. Ding, J. Xu, F. Da Ros, B. Huang, H. Ou, C. Peucheret, *Opt. Express* **2013**, *21*, 10376.
[38] D. Dai, J. Wang, Y. Shi, *Opt. Lett.* **2013**, *38*, 1422.
[39] M. Tomes, T. Carmon, *Phys. Rev. Lett.* **2009**, *102*, 11.
[40] K. Y. Song, Y. H. Kim, B. Y. Kim, *Opt. Lett.* **2013**, *38*, 1805.
[41] K. Y. Song, Y. H. Kim, *Opt. Lett.* **2013**, *38*, 4841.
[42] G. Bashan, Y. London, H. H. Diamandi, A. Zadok, *Optica* **2020**, *7*, 85.
[43] Y. Liu, A. Choudhary, G. Ren, D.-Y. Choi, A. Casas-Bedoya, B. Morrison, P. Ma, T. G. Nguyen, K. Vu, A. Mitchell, S. J. Madden, D. Marpaung, B. J. Eggleton, in *Conf. on Lasers and Electro-Optics*, Vol. 1, OSA, Washington, DC **2019**.
[44] M. S. Kang, A. Brenn, P. St.j.Russell, *Phys. Rev. Lett.* **2010**, *105*, 2.
[45] N. T. Otterstrom, R. O. Behunin, E. A. Kittlaus, Z. Wang, P. T. Rakich, *Science* **2018**, *360*, 1113.
[46] B. Shen, H. Lin, F. Merget, S. S. Azadeh, C. Li, G.-Q. Lo, K. A. Richardson, J. Hu, J. Witzens, *Opt. Express* **2019**, *27*, 13781.
[47] B. C. P. Sturmberg, K. B. Dossou, M. J. A. Smith, B. Morrison, C. G. Poulton, M. J. Steel, *J. Lightwave Technol.* **2019**, *37*, 3791.
[48] C. Wolff, M. J. Steel, C. G. Poulton, *Opt. Express* **2014**, *22*, 32489.
[49] W. Bogaerts, S. K. Selvaraja, *IEEE Photonics J.* **2011**, *3*, 422.
[50] D. B. Sohn, S. Kim, G. Bahl, *Nat. Photonics* **2018**, *12*, 91.
[51] D. Munk, M. Katzman, M. Hen, M. Priel, M. Feldberg, T. Sharabani, S. Levy, A. Bergman, A. Zadok, *Nat. Commun.* **2019**, *10*, 4214.
[52] E. A. Kittlaus, W. M. Jones, P. T. Rakich, N. T. Otterstrom, R. E. Muller, M. Rais-Zadeh, *Nat. Photonics* **2020**, *15*, 43.